JFM PAPERS

A pinned elastic plate on a thin viscous film

Philippe H. Trinh[1] , **Stephen K. Wilson**[1,2] **and Howard A. Stone**[3]

[1]Department of Mathematical Sciences, University of Bath, Claverton Down, Bath BA2 7AY, UK

[2]Department of Mathematics and Statistics, University of Strathclyde, Livingstone Tower, 26 Richmond Street, Glasgow G1 1XH, UK

[3]Department of Mechanical and Aerospace Engineering, Princeton University, Princeton, NJ 08544, USA

Corresponding author: Philippe H. Trinh, p.trinh@bath.ac.uk

Many problems in elastocapillary fluid mechanics involve the study of elastic structures interacting with thin fluid films in various configurations. In this work, we study the canonical problem of the steady-state configuration of a finite-length pinned and flexible elastic plate lying on the free surface of a thin film of viscous fluid. The film lies on a moving horizontal substrate that drives the flow. The competing effects of elasticity, viscosity, surface tension and fluid pressure are included in a mathematical model consisting of a third-order Landau–Levich equation for the height of the fluid film and a fifth-order Landau–Levich-like beam equation for the height of the plate coupled together by appropriate matching conditions at the downstream end of the plate. The properties of the model are explored numerically and asymptotically in appropriate limits. In particular, we demonstrate the occurrence of boundary-layer effects near the ends of the plate, which are expected to be a generic phenomenon for singularly perturbed elastocapillary problems.

1. Introduction

We study the steady-state configuration of a finite-length flexible elastic plate lying on the free surface of a thin film of viscous fluid which is itself lying on top of a horizontal substrate that is moving with constant speed. The upstream end of the plate is pinned at a fixed location and is in contact with a fluid reservoir. A typical configuration is shown in figure 1. We are particularly interested in the behaviour in the asymptotic limits of large

(*a*) $H(x)$ and $h(x)$

(*b*) $H_x(x)$ and $h_x(x)$
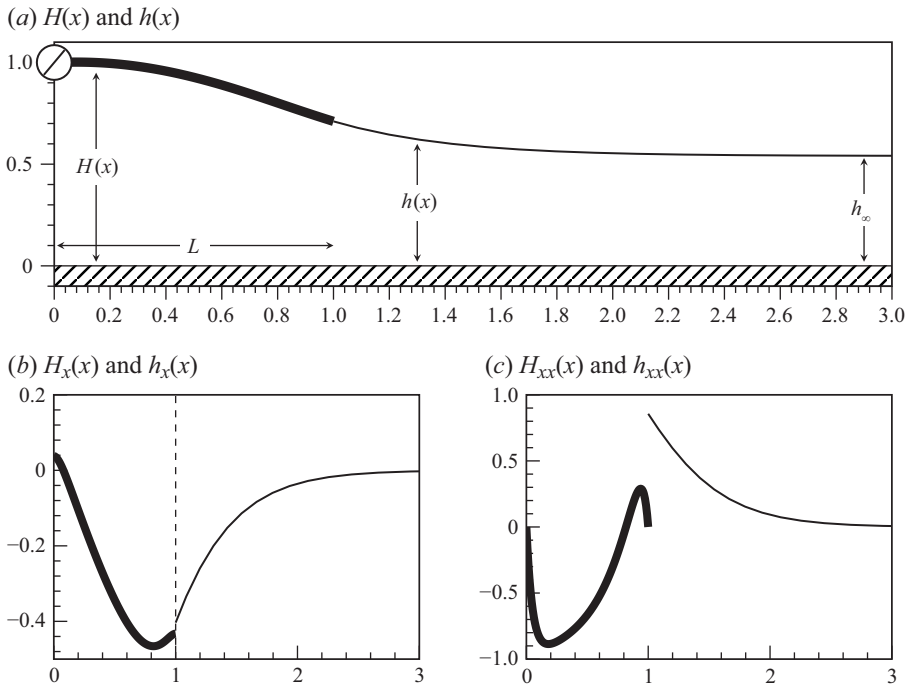
(*c*) $H_{xx}(x)$ and $h_{xx}(x)$

Figure 1. The numerically calculated heights of the elastic plate $H(x)$ (shown with the thick line) and the fluid film $h(x)$ (shown with the thin line). The horizontal axes correspond to x. The configuration corresponds to the case of the elasticity number $\mathcal{B} = 0.3$, inverse capillary number $\delta^3 = 1$, and prescribed pressure $p_0 = 1$. The heights are shown in (*a*), and their first and second derivatives are shown in (*b*) and (*c*), respectively. The numerical computation is explained in § 3.

and small dimensionless bending stiffness and of strong and weak surface tension (i.e. of slow and fast substrate motion, respectively).

As well as being of interest in its own right, this problem is a paradigm for a wide range of elastocapillary and fluid–structure interaction problems where competing effects of elasticity, viscosity, surface tension and fluid pressure can all play a role. Other examples of such problems, which involve elastocapillary and fluid–structure interaction effects, include the wetting of fibrous material studied, for example, by Bico *et al.* (2004), Duprat *et al.* (2012), Taroni & Vella (2012) and Singh *et al.* (2014), and recently reviewed by Duprat (2022). The dynamics of floating elastic sheets has been studied, for example, by Hosoi & Mahadevan (2004), Audoly (2011), Wagner & Vella (2011), Lister *et al.* (2013) and Hewitt *et al.* (2015). Perhaps closest to the present problem is the elastic drag-out problem studied, for example, by Pranckh & Scriven (1990), Giacomin *et al.* (2012), Dixit & Homsy (2013), Seiwert *et al.* (2013), and Snoeijer (2016). The authoritative review by Bico *et al.* (2018) gives an overview of recent developments in the study of elastocapillary effects.

We are particularly motivated by the previous work by Moriarty & Terrill (1996) and Trinh *et al.* (2014), who showed that even for the apparently simpler problem of a pinned or free-floating rigid plate, a variety of analytical and numerical challenges arise. For instance, the governing nonlinear boundary-value problem for the steady-state configurations can exhibit non-uniqueness, leading to a complicated bifurcation structure of the solution space. This previous work also demonstrates the challenges in obtaining accurate numerical solutions of coupled fluid–structure interaction problems of this kind,

particularly in asymptotic limits of strong and weak surface tension (i.e. of small and large capillary numbers, respectively). In such cases, asymptotic solutions may be necessary in order to obtain convergence in certain numerical schemes. In the present contribution, we build on this previous work to analyse the case of a flexible elastic, rather than rigid, plate. Again, the properties of the proposed mathematical model are explored numerically and analytically in appropriate asymptotic limits. In doing so, not only do we face many of the inherent challenges that appear in the case of a rigid plate, but we also encounter new difficulties that arise due to the singular effects of elasticity. In the Discussion, we consider various more complicated variations on the paradigm problem studied in the present work to which we expect that many of the elements of the present analysis will also be applicable.

More recently, there has been further investigation of this class of problems by Krapez *et al.* (2020) (see also Seiwert *et al.* 2013), who considered the spreading of a Newtonian fluid by a deformable, clamped blade. Physical experiments were conducted and scaling laws analysed in order to derive relationships between the wetted length of the blade and the downstream height of the film. This work has recently been extended to non-Newtonian fluids by Krapez *et al.* (2022). The present work provides a complementary analysis of the full mathematical model that goes beyond many of the (experimentally motivated) regimes studied in these works (see § 6 for further discussion).

We briefly introduce the model for the fluid film and the elastic plate; a complete derivation is given in § 2. The first equation is the well-known third-order Landau–Levich equation that describes the steady-state height of the fluid film $h = h(x)$. In non-dimensional form, it is given by

$$\delta^3 \frac{\mathrm{d}^3 h}{\mathrm{d}x^3} = \frac{3(h_\infty - h)}{h^3}, \tag{1.1}$$

where h_∞ is the uniform film height far downstream of the plate. The non-dimensional parameter δ^3 is an inverse capillary number, defined by

$$\delta^3 = \frac{\epsilon^3 \gamma}{\mu U} = \frac{1}{Ca}, \tag{1.2}$$

which represents the relative strength of the effects of surface tension γ and viscosity μ. Here, U is the speed of the substrate and $\epsilon \ll 1$ is the (small) aspect ratio of the thin film. Henceforth, for brevity, we use the phrase 'large and small limits of surface tension' as a shorthand for the more precise statement 'large and small limits of δ' (or equivalently, 'small and large limits of Ca').

The Landau–Levich equation (1.1) is a canonical equation in the study of coating and draining problems, and describes the steady-state configuration of a thin film of viscous fluid when the fluid and the substrate are in motion relative to each other. It was originally derived by Landau & Levich (1942) and Derjaguin (1943) to describe the drag-out problem, but variants of the equation occur in many other contexts. Examples include the propagation of long gas bubbles in a channel (see, for example, Bretherton 1961), coating fibres (see, for example, Quéré 1999), and coating the inside of a rotating cylinder (see, for example, Ashmore *et al.* 2003). Perhaps surprisingly, despite its widespread applicability, the full solution space of the Landau–Levich equation subject to a variety of different boundary conditions is still not well understood due to the non-uniqueness of solutions (see, for example, Snoeijer *et al.* 2008; Benilov *et al.* 2010; Ren *et al.* 2015). For further details of these and related problems, we refer readers to the works by Tuck & Schwartz (1990), Oron *et al.* (1997), de Gennes *et al.* (2004), Craster & Matar (2009) and Stone (2010).

The second equation, governing the height of the elastic plate $H = H(x)$, is a fifth-order Landau–Levich-like equation. In non-dimensional form, it is given by

$$\mathcal{B}^5 \frac{\mathrm{d}^5 H}{\mathrm{d}x^5} - \delta^3 \frac{\mathrm{d}^3 H}{\mathrm{d}x^3} = \frac{6(H - 2h_\infty)}{H^3}, \qquad (1.3)$$

and is a beam equation with additional terms incorporating tension and pressure effects due to the fluid underneath the plate. The non-dimensional parameter $\mathcal{B}$ is an elasticity number, defined by

$$\mathcal{B}^5 = \frac{\epsilon^3 B}{\mu U L^2}, \qquad (1.4)$$

which represents the relative strength of bending stiffness B and viscosity effects, where L is the length of the plate. Similarly to our description of δ mentioned earlier, henceforth we use the phrase 'small and large limits of bending stiffness' as a shorthand for 'small and large limits of $\mathcal{B}$'.

The model is closed by boundary conditions that couple (1.1) and (1.3) together at the downstream end of the plate, $x = L$, through continuity of the heights of the film and the plate, together with continuity of moment, shear and pressure forces. These will be described in further detail in § 2, and the numerical method used to solve the model will be described in § 3.

The subtleties inherent in the study of the coupled boundary-value problem are illustrated in figure 1, which shows a typical numerically calculated solution at a relatively small value of the elasticity number (specifically, $\mathcal{B} = 0.3$). In this example, we see that although the heights of the the plate and the fluid film are themselves well behaved, their derivatives are not. In particular, figures 1(*b*) and 1(*c*) show that there is a discontinuity in the first derivative at the downstream end of the plate and boundary layers in the second derivative at both ends of the plate, respectively. In § 4, we present a matched asymptotic analysis of the limits $\mathcal{B} \to \infty$ and $\mathcal{B} \to 0$, while in § 5, a similar analysis of the limits $\delta \to \infty$ and $\delta \to 0$ is performed. We emphasise that many of the mathematical features of the present work, notably the occurrence of boundary-layer effects illustrated in figure 1(*c*), are expected to be generic for elastocapillary systems in their singular limits. Indeed, as the present work demonstrates, solving elastocapillary and fluid–structure interaction problems of this kind can be a delicate affair, and a judicious combination of asymptotic and numerical techniques is often required in order to obtain the complete description.

2. Mathematical formulation

Let us consider steady, two-dimensional flow of a thin film of Newtonian fluid with constant density ρ, viscosity μ, and surface tension γ. The film lies on top of a rigid horizontal substrate, located at $\tilde{z} = 0$, that is moving to the right, i.e. in the positive $\tilde{x}$ direction, with constant speed U (see figure 1*a*). The free boundary of the fluid is composed of two parts: first, an elastic plate of projected length L located at

$$\tilde{z} = \tilde{H}(\tilde{x}) \quad \text{for } 0 < \tilde{x} < L, \qquad (2.1)$$

and second, an uncovered free surface located at

$$\tilde{z} = \tilde{h}(\tilde{x}) \quad \text{for } \tilde{x} > L, \qquad (2.2)$$

the latter of which has (unknown) uniform height h_∞ far downstream of the plate (i.e. as $\tilde{x} \to \infty$). In this work, we will consider the case in which the upstream end of the plate, located at $\tilde{x} = 0$, is pinned at a fixed height $\tilde{H}_0$, i.e. $\tilde{H}(0) = \tilde{H}_0$, where it is hinged and free

to rotate. The downstream end of the plate, located at $\tilde{x} = L$, is left free and its vertical position must be determined as part of the solution to the problem. The set-up is shown in figure 1(*a*). We note that it is, of course, possible to study other boundary conditions corresponding to different physical situations (for example, a clamped plate or the presence of a second free surface upstream of the plate), and these may introduce further subtleties.

The pressure and velocity of the fluid are denoted by $\tilde{p} = \tilde{p}(\tilde{x})$ and $\tilde{\boldsymbol{u}} = (\tilde{u}(\tilde{x}, \tilde{z}), \tilde{w}(\tilde{x}, \tilde{z}))$, respectively. The atmosphere above the film is assumed to be an inviscid fluid that is held at a uniform atmospheric pressure denoted by $\tilde{p}_a$. We non-dimensionalise and scale the variables according to

$$
\tilde{x} = Lx, \quad \tilde{z} = \epsilon Lz, \quad \tilde{H} = \epsilon LH, \quad \tilde{h} = \epsilon Lh,
$$
$$
\tilde{u} = Uu, \quad \tilde{w} = \epsilon Uw, \quad \tilde{p} - \tilde{p}_a = \frac{\mu U}{\epsilon^2 L}\, p, \tag{2.3}
$$

where $\epsilon = \tilde{H}_0/L \ll 1$ is the (small) aspect ratio of the film, given by the ratio of the fixed height of the upstream end of the plate to the length of the plate.

2.1. *The equation for the free surface*

To derive the equation governing the height of the free surface of the fluid, $z = h(x)$, we apply boundary conditions on the solid and free surfaces:

$$
\begin{array}{llll}
\text{no slip or penetration on substrate} & (u, w) = (1, 0) & \text{on} \quad z = 0, & (2.4a) \\
\text{no slip or penetration on plate} & (u, w) = (0, 0) & \text{on} \quad z = H(x), & (2.4b) \\
\text{normal stress balance on free surface} & p = -\delta^3 h_{xx} & \text{on} \quad z = h(x), & (2.4c) \\
\text{tangential stress balance on free surface} & u_z = 0 & \text{on} \quad z = h(x), & (2.4d)
\end{array}
$$

where $\delta^3 = \epsilon^3 \gamma/(\mu U) = 1/Ca$ is the non-dimensional inverse capillary number previously introduced in (1.2), and subscripts denote partial derivatives. Note that due to the thinness of the film, (2.4c) involves a linearised expression for the curvature of the free surface.

Classical lubrication (i.e. thin-film) theory now allows us to derive the Reynolds equation for the pressure gradient,

$$
p_x = \frac{3(h - h_\infty)}{h^3}, \tag{2.5}
$$

where $h \to h_\infty$ as $x \to \infty$. Substituting this expression for p_x into the normal stress condition (2.4c) yields the Landau–Levich equation

$$
\delta^3 h_{xxx} = \frac{3(h_\infty - h)}{h^3}, \tag{2.6}
$$

which governs the height of the free surface.

2.2. *The equation for the elastic plate*

Equation (2.6) for the height of the free surface must be coupled to an equation governing the height of the elastic plate, $z = H(x)$, which we now derive. First, let us consider the dimensional force per unit area exerted by the fluid on the plate, $\tilde{\boldsymbol{F}} = (\tilde{F}_{\tilde{x}}, \tilde{F}_{\tilde{z}})$. As in § 2.1, we make the lubrication approximation and assume that the plate is nearly horizontal.

Then the leading order in ϵ horizontal and vertical forces on the plate are given by

$$\tilde{F}_{\tilde{x}} = -\tilde{p}\frac{\mathrm{d}\tilde{H}}{\mathrm{d}\tilde{x}} + \mu\frac{\partial\tilde{u}}{\partial\tilde{z}} \quad \text{and} \quad \tilde{F}_{\tilde{z}} = \tilde{p}. \tag{2.7}$$

Let the dimensional tension in the plate be $\tilde{T} = \tilde{T}(\tilde{x})$. By balancing the horizontal forces we have $\mathrm{d}\tilde{T}/\mathrm{d}\tilde{x} = \tilde{F}_{\tilde{x}}$. Consideration of the surface tension at the end of the plate suggests a re-scaling of $\tilde{T} = \gamma T$, so using (2.3), we then have

$$\frac{\mathrm{d}T}{\mathrm{d}x} = \frac{\epsilon^2}{\delta^3}\left(-p\frac{\mathrm{d}H}{\mathrm{d}x} + \frac{\partial u}{\partial z}\right). \tag{2.8}$$

We assume that the aspect ratio is such that $\epsilon^2 \ll \delta^3 = 1/Ca$. Under this assumption, the tension is constant at leading order in ϵ, thus the balance with surface tension at the end of the plate implies that $T \equiv 1$.

We let $\tilde{N} = \tilde{N}(\tilde{x})$ be the dimensional transverse shear force and let $\tilde{M} = \tilde{M}(\tilde{x})$ be the dimensional moment. The normal force and moment balances on the elastic plate are given, respectively, by

$$\frac{\mathrm{d}\tilde{N}}{\mathrm{d}\tilde{x}} + \tilde{T}\frac{\mathrm{d}^2\tilde{H}}{\mathrm{d}\tilde{x}^2} + \tilde{p} = 0, \tag{2.9a}$$

$$\frac{\mathrm{d}\tilde{M}}{\mathrm{d}\tilde{x}} = \tilde{N} \tag{2.9b}$$

(see, for example, Howell *et al.* 2009). Furthermore, for small displacements, we assume the constitutive relation

$$\tilde{M} = -B\frac{\mathrm{d}^2\tilde{H}}{\mathrm{d}\tilde{x}^2}, \tag{2.10}$$

where $B = EI$ is the bending stiffness, in which E is the elastic modulus and I is the area moment of inertia. Recalling that $T \equiv 1$, we now differentiate (2.4c) with respect to $\tilde{x}$, and use (2.3), the Reynolds equation (2.5), the constitutive relation (2.10), and $T \equiv 1$ to obtain the equation governing the height of the plate, namely

$$\mathcal{B}^5\frac{\mathrm{d}^5H}{\mathrm{d}x^5} - \delta^3\frac{\mathrm{d}^3H}{\mathrm{d}x^3} = \mathcal{R}(H; h_\infty), \tag{2.11}$$

where, for later convenience, we have defined the function

$$\mathcal{R}(H; h_\infty) = \frac{6(H - 2h_\infty)}{H^3}, \tag{2.12}$$

and $\mathcal{B}^5 = \epsilon^3 B/(\mu U L^2)$ is the non-dimensional elasticity number previously introduced in (1.4).

Turning now to the boundary conditions at the pinned ($x = 0$) and free ($x = 1$) ends of the plate, we recall that from the constitutive relation (2.10), the moment is proportional to the second derivative of H, hence

$$H(0) = 1, \tag{2.13a}$$

$$H_{xx}(0) = 0 = H_{xx}(1). \tag{2.13b}$$

In light of the fact that the free surface exerts a tangential force due to surface tension at the downstream end of the plate, $x = 1$, the zero moment condition (2.13b) is not obvious. We will discuss this condition further in § 2.3.
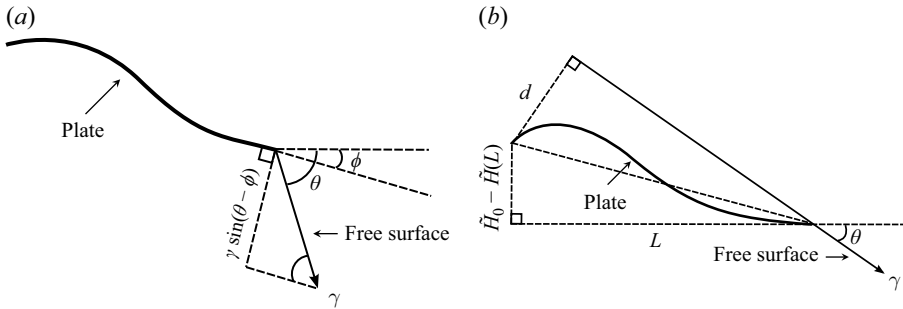
Figure 2. (*a*) Quantities defined near the downstream end of the plate. (*b*) An illustration of the moment arm due to surface tension forces.

Examining figure 2(*a*), which shows quantities defined near the downstream end of the plate, we see that a balance of shear stress at the end of the plate, $x = 1$, implies the dimensional balance

$$\tilde{N}(L) + \tilde{T}\big[\tilde{H}_{\tilde{x}}(L) - \tilde{h}_{\tilde{x}}\big] = 0, \tag{2.14}$$

so using (2.3), (2.9*b*) and (2.10) gives the shear boundary condition

$$\mathcal{B}^5 H_{xxx}(1) - \delta^3 \left[H_x(1) - h_x(1)\right] = 0. \tag{2.15}$$

Without loss of generality, we take $\tilde{p}_a \equiv 0$. Then the upstream fluid pressure must match the prescribed pressure of the reservoir, $p_0 \equiv p(0)$, and similarly, the pressure of the fluid at the downstream end of the plate must match the capillary pressure $-\delta^3 h_{xx}(1)$. Since the pressure underneath the plate is given by (2.9*a*), or alternatively the integral of (2.11), the non-dimensional pressure under the plate is given by

$$p = \mathcal{B}^5 H_{xxxx} - \delta^3 H_{xx}. \tag{2.16}$$

Then applying the boundary conditions gives

$$\mathcal{B}^5 H_{xxxx}(0) = p_0, \tag{2.17a}$$

$$\mathcal{B}^5 H_{xxxx}(1) = -\delta^3 h_{xx}(1). \tag{2.17b}$$

Finally, we require additional details of the far-field behaviour, $h \to h_\infty$ as $x \to \infty$. We linearise about the uniform downstream height by writing $h = h_\infty + \overline{h}$, where $\overline{h} \ll h_\infty$. The resulting modes of the linear equation for h_∞ can be obtained using a standard WKBJ (Liouville–Green) analysis (see, for example, Tuck & Schwartz 1990) to yield

$$\overline{h} \sim C_1 \exp\left(-\frac{3^{1/3}x}{\delta h_\infty}\right) + C_2 \exp\left(\frac{3^{1/3}\mathrm{e}^{\pi i/3}x}{\delta h_\infty}\right) + C_3 \exp\left(\frac{3^{1/3}\mathrm{e}^{-\pi i/3}x}{\delta h_\infty}\right) \tag{2.18}$$

as $x \to \infty$, where C_1 is real and C_2 and C_3 are complex conjugates. The two exponentially growing modes, which represent capillary waves, are ruled out on physical grounds, so that $C_2 = 0$ and $C_3 = 0$, leaving only C_1 to be determined. Thus we see that, as is typical for problems of this type, the downstream condition $h \to h_\infty$ effectively provides two boundary conditions for the third-order Landau–Levich equation (2.6). This completes our derivation of the governing equations and boundary conditions.

2.3. *Summary and remarks on the non-trivial nature of the mathematical formulation*

Together, we may consider the system of equations and boundary conditions for the pinned elastic problem to correspond to a 'ninth-order' problem; the relevant expressions

Unknowns	Equations	Boundary conditions
$h(x)$, $H(x)$, h_∞	$\delta^3 h_{xxx} = 3(h_\infty - h)/h^3$ $\mathcal{B}^5 H_{xxxxx} - \delta^3 H_{xxx} = 6(H - 2h_\infty)/H^3$	[1] $H(0) = 1$ [2] $H_{xx}(0) = 0$ [3] $\mathcal{B}^5 H_{xxxx}(0) = p_0$ [4] $H(1) = h(1)$ [5] $H_{xx}(1) = 0$ [6] $\mathcal{B}^5 H_{xxx}(1) - \delta^3[H_x(1) - h_x(1)] = 0$ [7] $\mathcal{B}^5 H_{xxxx}(1) = \delta^3 h_{xx}(1)$ [8,9] $h \to h_\infty$ as $x \to \infty$

Table 1. A summary of the 'ninth-order' system of equations and boundary conditions for the pinned elastic problem analysed in the present work, comprising a third-order equation for h, a fifth-order equation for H, and an unknown 'eigenvalue' h_∞.

are given in table 1. In particular, the system consists of the third-order Landau–Levich equation for $h(x)$, the fifth-order beam equation for $H(x)$, and an unknown eigenvalue corresponding to the far-field film height h_∞. In total, this system requires nine boundary conditions. These nine boundary conditions consist of: [1, 2, 3] fixed height, zero moment, and prescribed pressure at $x = 0$; [4, 5, 6, 7] continuity of height, zero moment, continuity of shear stress and pressure at $x = 1$; and [8, 9] far-field conditions as $x \to \infty$.

Although we have chosen to derive the governing equations and boundary conditions using local force and moment balances, we note that it is also possible to use a variational approach. Using the small displacement and lubrication approximations, we see that the equilibrium configuration of the plate should extremise the dimensional energy:

$$\mathcal{E} = \int_0^L \left\{ \underbrace{\frac{1}{2}\mathcal{B}\tilde{H}_{\tilde{x}\tilde{x}}^2}_{\text{bending energy}} - \underbrace{\tilde{p}\tilde{H}}_{\text{pressure energy}} + \underbrace{\tilde{T}\left[\sqrt{1 + \tilde{H}_{\tilde{x}}^2} - 1\right]}_{\text{tension energy}} \right\} d\tilde{x}$$

$$+ \int_L^\infty \left\{ \underbrace{\gamma\left[\sqrt{1 + \tilde{h}_{\tilde{x}}^2} - 1\right]}_{\text{surface tension energy}} - \underbrace{\tilde{p}\tilde{h}}_{\text{pressure energy}} \right\} d\tilde{x}. \tag{2.19}$$

It can then be verified that the equations and boundary conditions given in table 1 can be recovered if we require that the first variation of $\mathcal{E}$ given by (2.19) is zero.

We make some remarks about the non-trivial nature of the mathematical formulation just presented. In the statement of the zero moment condition (2.13*b*), we indicated that it is not entirely obvious that this condition guarantees that the plate is in rotational equilibrium. Although the conditions emerge naturally from application of the variational approach described above, we can directly verify that the dimensional moment about $\tilde{x} = 0$ is zero, i.e. $\tilde{M}_0 = 0$. This moment has a pressure contribution and a contribution from surface tension forces, and is given by

$$\tilde{M}_0 = \gamma d + \int_0^L \tilde{x}\, \tilde{p}(\tilde{x})\, d\tilde{x}, \tag{2.20}$$

where d is the length of the moment arm due to the surface tension forces (i.e. the perpendicular distance from $(0, \tilde{H}_0)$ to the line parallel to the tension force), as shown

in figure 2(*b*). For small displacements of the plate, this distance is given by

$$d \sim L \left[\tilde{h}_{\tilde{x}}(L) + \frac{\tilde{H}_0 - \tilde{H}(L)}{L} \right]. \tag{2.21}$$

We may now substitute the dimensional version of the pressure under the plate given by (2.16) into (2.20), integrate by parts, and simplify using the boundary conditions at $\tilde{x} = 0$ and $\tilde{x} = L$, to confirm that $\tilde{M}_0 = 0$.

3. Numerical method

We solve the system given in table 1 numerically using finite difference and collocation methods. The solution space is then explored using numerical continuation techniques. It is often the case that finding an initial solution (or continuing a solution near a singular limit) is difficult; thus in order to provide an initial solution, we used either the asymptotic solutions of Trinh *et al.* (2014) (for which $\mathcal{B} = 0$) or the asymptotic solutions obtained in §§ 4 and 5 for large and small values of the parameters $\mathcal{B}$ and δ.

For given values of $\mathcal{B}$, δ and p_0, the fifth-order boundary-value problem for $H(x)$ is solved with h_∞ as an unknown eigenvalue. However, imposition of the six boundary conditions [1–3, 5–7] given in table 1 requires values of $h_x(1)$ and $h_{xx}(1)$. Thus for each iteration of the boundary-value problem, we must solve the Landau–Levich equation (2.6). The procedure is as follows.

(i) Set fixed values of the parameters $\mathcal{B}$, δ and p_0.
(ii) Given an approximate value for $H(1)$ (set to $\hat{H}(1)$).
    (*a*) Solve the Landau–Levich equation (2.6) for $h(x)$ as an initial-value problem from $x_{max} \gg 1$ backwards to $x = 1$. Stop once $h(1) = \hat{H}(1)$ is reached. Collect the values of $h_x(1)$ and $h_{xx}(1)$.
    (*b*) Solve the beam equation (2.11) as a boundary-value problem for $H(x)$ and h_∞. Collect the (incorrect) value of $H(1)$ (set to $\tilde{H}(1)$).
(iii) Set $R = \hat{H}(1) - \tilde{H}(1)$. Iterate a Newton-type solver for $R = 0$ in order to determine the correct value of $H(1)$.

In step (ii,*a*) we begin from an initial height $h = h_\infty + \varepsilon$, where ε is a small number (specifically, $\varepsilon = 10^{-12}$ in most computations). The far-field behaviour (2.18) (with $C_2 = C_3 = 0$) provides values of the first and second derivatives, thus the Landau–Levich equation can be solved in the negative x direction as an initial-value problem, stopping once $h = \hat{H}(1)$ is reached. Once the Landau–Levich equation has been solved, the approximate values of $h_x(1)$ and $h_{xx}(1)$ are known (for an, in general, incorrect value of $H(1)$), and the system is closed. Hence there are six boundary conditions for the fifth-order beam equation, with $H(1)$ serving as an unknown eigenvalue.

An example solution with positive prescribed pressure $p_0 = 1$ has already been shown in figure 1. An example with negative prescribed pressure $p_0 = -0.5$ is shown in figure 3.

4. Asymptotic analysis of large and small bending stiffness $\mathcal{B}$

In this section, we study the system given in table 1 in the limits of large ($\mathcal{B} \to \infty$) and small ($\mathcal{B} \to 0$) bending stiffness. Although the limit $\mathcal{B} \to 0$ has no analogue in our previous work, we would anticipate that in the limit $\mathcal{B} \to \infty$ we will recover the behaviour of a rigid plate described by Trinh *et al.* (2014). While this turns out to be the case, the
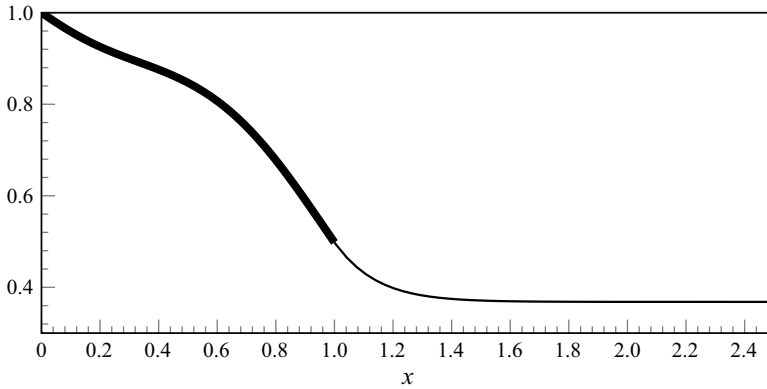
Figure 3. The heights of the elastic plate $H(x)$ (shown with the thick line) and the fluid film $h(x)$ (shown with the thin line) in the case $\mathcal{B} = 0.3$, $\delta = 0.5$ and $p_0 = -0.5$.

more interesting phenomenon is how the addition of small but non-zero elasticity affects the equilibrium configuration.

4.1. *The limit of a rigid plate, $\mathcal{B} \to \infty$*

In the limit of a rigid plate, $\mathcal{B} \to \infty$, we assume that there are no boundary layers (notably no boundary layers at $x = 0$ and/or $x = 1$), and expand the free surface and plate heights and the far-field film height as

$$h(x) = \sum_{n=0}^{\infty} \frac{h_n(x)}{\mathcal{B}^{5n}}, \quad H(x) = \sum_{n=0}^{\infty} \frac{H_n(x)}{\mathcal{B}^{5n}} \quad \text{and} \quad h_\infty = \sum_{n=0}^{\infty} \frac{h_{\infty n}}{\mathcal{B}^{5n}}. \tag{4.1}$$

At leading order, the beam equation (2.11), together with the boundary conditions $H_0(0) = 1$ and $H_{0xx}(0) = 0$, yields a solution for $H_0 = H_0(x)$ corresponding to a straight (but not, in general, horizontal) rigid plate, namely

$$H_0 = 1 + \alpha x, \tag{4.2}$$

where the constant α is the unknown tilt angle. What is noteworthy about this solution is that in order to obtain the values of α and h_∞, the moment and force balances must be applied at $\mathcal{O}(1/\mathcal{B}^5)$. This occurs because while for a rigid plate, the curvature (and all higher-order derivatives) of H are identically zero, for an elastic plate, these higher-order derivatives are non-zero and are essential in order to satisfy the boundary conditions.

At $\mathcal{O}(1/\mathcal{B}^5)$, (2.11) yields

$$H_{1xxxxx} - \delta^3 H_{0xxx} = \frac{6}{H_0^3}(H_0 - 2h_{\infty 0}). \tag{4.3}$$

Integrating (4.3) from $x = 0$ to $x = 1$, and using the zero moment (2.13*b*) and pressure (2.17) boundary conditions yields the leading-order shear condition

$$F_z^{(0)} = p_0 + \delta^3 h_{xx}(1) + [6 I_2(1) - 12h_{\infty 0} I_3(1)] = 0, \tag{4.4}$$

where we have introduced the notation

$$I_k(x) \equiv \int_0^x \frac{1}{H_0^k(x')} \, dx'. \tag{4.5}$$

In fact, the shear condition (4.4) was obtained by Trinh *et al.* (2014) for a rigid plate (their (2.15)), but with our leading-order H_0 replaced by their full expression for $H(x)$. Thus (4.4) is a leading-order shear condition, $F_z \sim F_z^{(0)}$, valid in the limit $\mathcal{B} \to \infty$. Since there are two remaining unknowns, namely α and $h_{\infty 0}$, to be determined at $\mathcal{O}(1)$, we expect to complement (4.4) with an additional equation expressing a moment balance. Integrating (4.3) three times and using the zero moment conditions (2.13*b*) yields

$$
H_{1xx}(x) - H_{1xxxx}(0)\left[\frac{x^2}{2} - x\right] - x\, H_{1xxx}(1) + \delta^3\left[H_{0x}(1) - \{H_0(x) - H_0(0)\}\right]
$$
$$
= \int_0^x \int_1^{x_2} [6\, I_2(x_1) - 12 h_{\infty 0}\, I_3(x_1)]\, \mathrm{d}x_1 \mathrm{d}x_2. \tag{4.6}
$$

Setting $x = 1$ in (4.6), reversing the order of integration, and applying the boundary conditions (2.15), (2.17) and the expression for the height of a rigid plate (4.2), we obtain a leading-order zero moment condition,

$$
M_0^{(0)} = \frac{p_0}{2} + \delta^3\left[h_{0x}(1) - \alpha\right] + \int_0^1 [6x\, I_2(x_1) - 12 h_{\infty 0} x_1\, I_3(x_1)]\, \mathrm{d}x_1 = 0, \tag{4.7}
$$

which coincides with the corresponding expression obtained by Trinh *et al.* (2014) (their (3.5)). Our (4.7), however, is a leading-order moment condition $M_0 \sim M_0^{(0)}$, valid in the limit $\mathcal{B} \to \infty$.

In summary, we have demonstrated that the behaviour in the limit of a rigid plate $\mathcal{B} \to \infty$ is nearly the same as that when elasticity is entirely ignored. However, when elasticity is included and $\mathcal{B}$ is large but finite, the plate is not quite flat, but is gently curved with $\mathcal{O}(1/\mathcal{B}^5)$ curvature. The determination of the final two unknowns requires the solution of the third-order Landau–Levich equation (2.6), subject to two far-field conditions ([8, 9] given in table 1), the continuity condition $h_0(1) = H_0(1) = 1 + \alpha$, the shear condition (4.4), and the moment condition (4.7). Although this can be done numerically, asymptotic formulae in the limits $\delta \to 0$ and $\delta \to \infty$ were derived by Trinh *et al.* (2014). For instance, in the limit $\delta \to \infty$,

$$
\alpha \sim \frac{p_0 - 6}{3^{1/3}\delta^2} \quad \text{and} \quad h_{\infty 0} \sim 1 + \frac{p_0 - 6}{3^{2/3}\delta}, \tag{4.8}
$$

while the limit of $\delta \to 0$ is more complicated because of the existence of possibly more than one solution due to the effects of the prescribed pressure, p_0.

In figure 4, we present the far-field film height h_∞ as a function of δ for values of $\mathcal{B}$ ranging from $\mathcal{B} = 0.1$ to $\mathcal{B} = 1$. In particular, figure 4 shows that by $\mathcal{B} = 1$, the far-field film height is nearly identical to the leading-order asymptotic solution in the limit $\mathcal{B} \to \infty$, obtained from numerical solutions of the problem for a rigid plate.

4.2. *The limit of a very flexible plate, $\mathcal{B} \to 0$*

We now study the limit of a very flexible plate, $\mathcal{B} \to 0$. In fact, the asymptotic solution in this limit turns out to be very useful because the numerical solution of the governing boundary-value problem becomes increasingly (mathematically) stiff as the plate becomes increasing (physically) flexible. We expand the (outer) solution as

$$
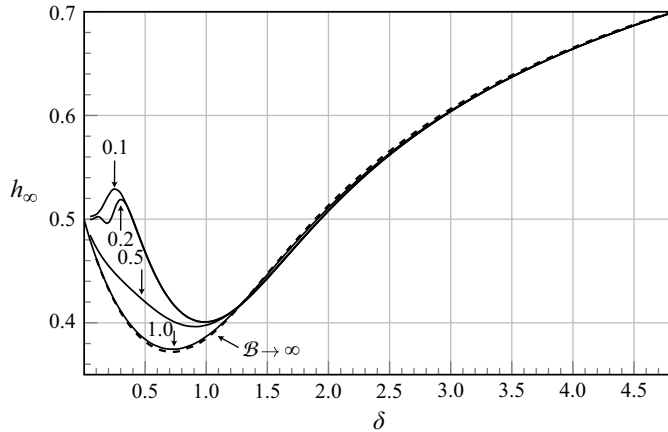H(x) \sim H_{outer}(x) = \sum_{n=0}^{\infty} \mathcal{B}^n H_n, \tag{4.9}
$$

Figure 4. The far-field film height h_∞ plotted as a function of δ for various values of $\mathcal{B}$ in the case $p_0 = 0$. From top to bottom, the curves correspond to $\mathcal{B} = 0.1, 0.2, 0.5$ and 1.0. The leading-order asymptotic solution in the limit of a rigid plate $\mathcal{B} \to \infty$ described in § 4.1 is shown with the dashed line.

with similar expansions for $h(x) \sim h_0(x)$ and $h_\infty \sim h_{\infty 0}$. From (2.11), the equation for the leading-order (outer) plate height is

$$-\delta^3 H_{0xxx} \sim \mathcal{R}(H_0; h_\infty), \tag{4.10}$$

so we need to provide four boundary conditions at $x = 0$ and $x = 1$.

We find a rather complicated boundary-layer structure in this singular limit. We will begin by considering the simpler case of zero prescribed pressure $p_0 = 0$, and then return to the case of general values of p_0 in § 4.2.5. When $p_0 = 0$, numerically calculated solutions of the problem for small values of $\mathcal{B}$ indicate that there is no boundary layer near $x = 0$, thus we can apply the conditions $H(0) = 1$ and $H_{xx}(0) = 0$ there. The remaining three conditions must be selected from amongst the four conditions [3, 5, 6, 7] given in table 1, and the challenge is to determine which ones. As it turns out, the outer solution, valid away from $x = 1$, is coupled to inner solutions near $x = 1$ via three nested boundary layers.

The full beam equation involves contributions from the elasticity, surface tension and pressure. We write

$$\underbrace{\mathcal{B}^5 H_{xxxxx}}_{\text{①}} - \underbrace{\delta^3 H_{xxxx}}_{\text{②}} = \underbrace{\mathcal{R}(H; h_\infty)}_{\text{③}}, \tag{4.11}$$

and define the following regions and asymptotic balances.

Outer	$x - 1 = \mathcal{O}(1)$		where ② $\sim$ ③,	(4.12a)
Region I	$x - 1 = \mathcal{O}(\mathcal{B}^\alpha)$	for $\alpha < 5/2$	where ① $\ll$ ②,	(4.12b)
Region II	$x - 1 = \mathcal{O}(\mathcal{B}^{5/2})$		where ① $\sim$ ②,	(4.12c)
Region III	$x - 1 = \mathcal{O}(\mathcal{B}^\alpha)$	for $\alpha > 5/2$	where ① $\gg$ ②.	(4.12d)

In the outer region, surface tension balances the contribution from pressure forces. Moving towards the inner region near $x = 1$, first the outermost boundary layer (region I) in which surface tension dominates elasticity is encountered, then the intermediate boundary layer (region II) in which surface tension and elasticity balance, and finally the innermost boundary layer (region III) in which elasticity dominates.
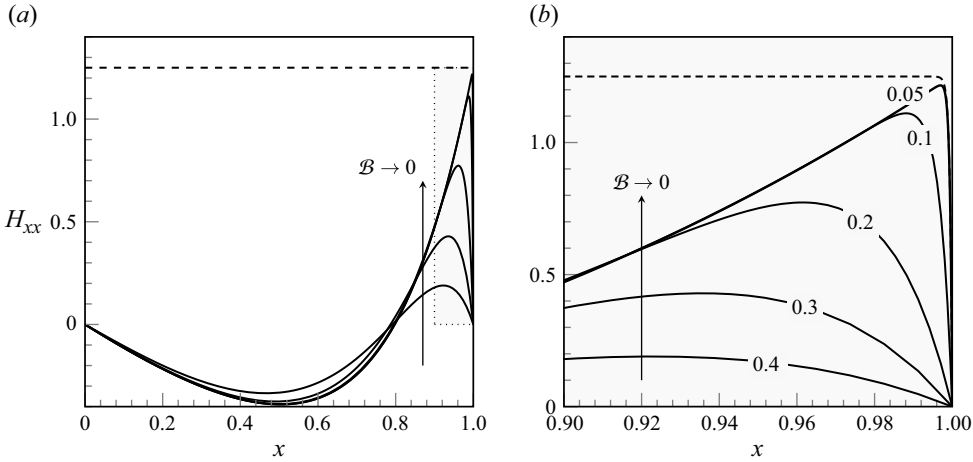
Figure 5. The curvature of the plate H_{xx} plotted as a function of x for various values of $\mathcal{B}$ in the case $\delta = 1$ and $p_0 = 1$. From top to bottom on the right, the curves correspond to $\mathcal{B} = 0.05, 0.1, 0.2, 0.3$ and 0.4. The asymptotic solution in region II given by (4.23b) is shown with the dashed line. Plot (b) is an enlargement of plot (a) near $x = 1$.

Before we present the analysis of this inner region, we display in figure 5 typical profiles of the curvature of the plate, $H_{xx}(x)$, calculated from the numerical solutions of the full system in the case $p_0 = 1$. The reason for examining H_{xx} (rather than H or H_x) is that the boundary layers appear only in the second and higher derivatives of the leading-order terms. Crucially, the numerical solutions indicate that

$$H(x), \ H_x(x) \text{ and } H_{xx}(x) \text{ are all bounded and non-zero as } \mathcal{B} \to 0 \tag{4.13}$$

for fixed values of δ and fixed $x \in (0, 1)$.

Based on figure 5, we see that although the zero moment condition (2.13b) requires $H_{xx}(1) = 0$, the leading-order solution in the outer region has a curvature that approaches a non-zero value as $x \to 1$. Our principal task is to determine this effective value of the curvature, shown with the dashed line in figure 5, which provides a boundary condition on the outer solution.

4.2.1. *Region II: elasticity and surface tension balance*

We begin in region II, where elasticity ① balances surface tension ②. Solving the leading-order equation $\mathcal{B}^5 H_{xxxxx} \sim \delta^3 H_{xxx}$ gives

$$H_{xxx}^{\mathrm{II}} \sim A \exp\left[-\frac{\delta^{3/2}}{\mathcal{B}^{5/2}}(1-x)\right] + \hat{A} \exp\left[\frac{\delta^{3/2}}{\mathcal{B}^{5/2}}(1-x)\right], \tag{4.14}$$

where A and $\hat{A}$ are constants (possibly dependent on $\mathcal{B}$ and δ). We assume that $\hat{A} = 0$, as this suppresses the otherwise unmatchable exponential growth. Integrating (4.14) once yields

$$H_{xx}^{\mathrm{II}} \sim \frac{A\mathcal{B}^{5/2}}{\delta^{3/2}} \exp\left[-\frac{\delta^{3/2}}{\mathcal{B}^{5/2}}(1-x)\right] + C, \tag{4.15}$$

where C is constant. However, note from the assumption (4.13) that the curvature is bounded and non-zero, so $A = \mathcal{O}(\mathcal{B}^{-5/2})$ and $C = \mathcal{O}(1)$. We therefore re-scale the

constants A and C and write (4.15) as

$$H_{xx}^{\mathrm{II}} \sim \frac{\tilde{A}}{\delta^{3/2}} \exp\left[-\frac{\delta^{3/2}}{\mathcal{B}^{5/2}}(1-x)\right] + \tilde{C}, \tag{4.16}$$

where $\tilde{A}$ and $\tilde{C}$ are $\mathcal{O}(1)$.

In region III, we assume the scaling $1 - x = \mathcal{B}^{\alpha}s$ for $\alpha > 5/2$ and $s = \mathcal{O}(1)$. Thus if we take x from region II to region III, then within the exponential argument, $(1-x)/\mathcal{B}^{5/2} = \mathcal{B}^{-(5/2-\alpha)}s$, and this quantity must be small. Consequently, we may expand

$$H_{xx}^{\mathrm{II} \to \mathrm{III}} \sim \frac{\tilde{A}}{\delta^{3/2}} - \frac{\tilde{A}(1-x)}{\mathcal{B}^{5/2}} + \mathcal{O}\left(\frac{(1-x)^2}{\mathcal{B}^{10/2}}\right) + \tilde{C}. \tag{4.17}$$

From the zero moment condition (2.13b), we require $H_{xx}(1) = 0$. We make the assumption (which can be verified *a posteriori*) that this applies even for the inner limit of the region II solution, thus

$$\tilde{C} = -\frac{\tilde{A}}{\delta^{3/2}}. \tag{4.18}$$

Proceeding now in the other direction, and studying the transition from region II to region I, we find that

$$H_{xx}^{\mathrm{II} \to \mathrm{I}} \sim -\frac{\tilde{A}}{\delta^{3/2}} + \text{ exponentially small terms in } \frac{\delta^{3/2}(1-x)}{\mathcal{B}^{5/2}}, \tag{4.19}$$

once we have made the substitution (4.18). Thus the curvature is effectively constant to all algebraic orders, and it is precisely this constant, namely $\tilde{C} = -\tilde{A}/\delta^{3/2}$, that is shown with the dashed line in figure 5.

4.2.2. *Region I: surface tension dominates elasticity and pressure*

In region I, we have $\delta^3 H_{xxx} \ll 1$, which gives $H_{xx}^{\mathrm{I}} \sim$ constant. This solution must match (4.19), so the constant must be equal to (4.18), thus

$$H_{xx}^{\mathrm{II}} = -\frac{\tilde{A}}{\delta^{3/2}}. \tag{4.20}$$

4.2.3. *Region III: elasticity dominates surface tension and pressure*

Let us consider the solution in the innermost region III, where elasticity ① dominates both surface tension ② and pressure ③. In this case, we have $H_{xxxxx} \ll 1$, so integrating three times yields

$$H_{xx}^{\mathrm{III}} \sim \frac{C_A}{2}(1-x)^2 + C_B(1-x) + C_C, \tag{4.21}$$

for new constants C_A, C_B and C_C. From the zero moment condition (2.13b), $H_{xx}(1) = 0$, thus $C_C = 0$. Based on the $H^{\mathrm{II} \to \mathrm{III}}$ limit of (4.17), we argue that the solution in region III cannot diverge quadratically as x moves away from $x = 1$, and consequently $C_A = 0$. Then we match (4.17) and (4.21) to obtain

$$C_B = -\frac{\tilde{A}}{\mathcal{B}^{5/2}}. \tag{4.22}$$

4.2.4. *Summary and final matching*

At this point, we have the following solutions:

$$H_{xx}^{\mathrm{I}} \sim -\frac{\tilde{A}}{\delta^{3/2}}, \tag{4.23a}$$

$$H_{xx}^{\mathrm{II}} \sim \frac{\tilde{A}}{\delta^{3/2}} \exp\left[-\frac{\delta^{3/2}(1-x)}{\mathcal{B}^{5/2}}\right] - \frac{\tilde{A}}{\delta^{3/2}}, \tag{4.23b}$$

$$H_{xx}^{\mathrm{III}} \sim -\frac{\tilde{A}(1-x)}{\mathcal{B}^{5/2}}. \tag{4.23c}$$

We now apply the remaining boundary conditions. Since $\mathcal{B}^5 H_{xxx}(1) = \mathcal{O}(\mathcal{B}^{5/2})$ according to the solution in region III (or region II), the shear condition (2.15) reduces to $H_x(1) \sim h_x(1)$ at leading order. Thus in the limit $\mathcal{B} \to 0$ the plate and free surface contact tangentially. The pressure condition (2.17b) applied to the inner limit of the solution in region II (4.23b) indicates that

$$\mathcal{B}^5 H_{xxxx}(1) \sim \mathcal{B}^5 \frac{\tilde{A}}{\delta^{3/2}}\left(\frac{\delta^{3/2}}{\mathcal{B}^{5/2}}\right)^2 = \tilde{A}\delta^{3/2} = -\delta^3\, h_{xx}(1), \tag{4.24}$$

thus we have determined the final constant to be

$$\tilde{A} = -\delta^{3/2}\, h_{xx}(1). \tag{4.25}$$

Substitution of this value of $\tilde{A}$ into (4.23a) gives the effective value of the curvature to be applied as a boundary condition on the outer solution, namely $H_{xx}(1) = h_{xx}(1)$.

In summary, in order to determine the leading-order outer solution in the limit $\mathcal{B} \to 0$, we solve the outer boundary-value problem

$$-\delta^3 H_{xxx} = \mathcal{R}(H; h_\infty), \tag{4.26a}$$

$$H(0) = 1, \quad H_{xx}(0) = 0, \tag{4.26b}$$

$$H(1) = h(1), \quad H_x(1) = h_x(1), \quad H_{xx}(1) = h_{xx}(1), \tag{4.26c}$$

in the following way. First, values of h_∞ and $H(1)$ are used as initial guesses. The Landau–Levich equation (2.6) is solved starting at a large value of $x = x_{\max} \gg 1$, with h close to its far-field value, and stopping once $h = H(1)$. At this point, we solve the third-order boundary-value problem (4.26a) subject to three of the five conditions (4.26b) and (4.26c). The shooting algorithm is then repeated to converge to the correct values of h_∞ and $H(1)$ in order to satisfy the remaining two conditions.

It is a curious fact that the effective boundary conditions on the outer problem, namely (4.26), impose the constraint that the elastic plate, $H(x)$, and the free surface, $h(x)$, are continuous in their heights, derivatives and curvatures. As a consequence, the plate and the film behave very similarly to a fluid with an uncovered free surface. However, we should recall that the equation for $H(x)$ imposes a zero-slip condition on the free surface, whereas the velocity profiles for $h(x)$ will exhibit slip at the free surface. Additionally, the interpretation of the elastic plate as continuously attaching to the fluid is true only of the outer solution, as is shown clearly in figure 5. In particular, there is a rapid variation in the curvature of the elastic plate from its non-zero effective value (proportional to the curvature $h_{xx}(x)$) to the zero value required for the zero moment condition.

4.2.5. *Modification for $p_0 \neq 0$*

Now that we have understood the nested boundary-layer structure of the inner region, we see that the introduction of regions I and III is not strictly necessary in order to derive the effective boundary conditions on the outer problem. This is because the solution in the intermediate region (region II) contains the information about all three boundary-layer regions, and in fact, the boundary conditions exactly at $x = 1$ can be applied directly to the solution in region II. The crucial quality that allows for this is that the terms that change balance between regions I, II and III are exponential in nature.

With the introduction of $p_0 \neq 0$, another boundary layer (or, more accurately, three new boundary layers) must be introduced in a new inner region near $x = 0$. Using the same naming convention for the three regions, the solution in the intermediate region, where the dominant balance is $\mathcal{B}^5 H_{xxxxx} \sim \delta^3 H_{xxx}$, has the curvature

$$H_{xx}^{\text{II, left}} \sim \frac{a_1}{\delta^{3/2}} \exp\left(-\frac{\delta^{3/2}}{\mathcal{B}^{5/2}} x\right) + a_2, \qquad (4.27)$$

where, as in § 4.2.1, we have scaled the constants a_1 and a_2 so that the curvature remains non-zero as in the limit $\mathcal{B} \to 0$. Next, matching with the innermost solution, II $\to$ III requires that $H_{xx}(0) = 0$ for the hinged plate. Thus $a_2 = -a_1/\delta^{3/2}$. The last step is to apply the pressure condition (2.17a), requiring $\mathcal{B}^5 H_{xxxx}(0) = p_0$; this gives $a_1 = p_0/\delta^{3/2}$, so the final intermediate solution is

$$H_{xx}^{\text{II, left}} \sim \frac{p_0}{\delta^3} \left[\exp\left(-\frac{\delta^{3/2}}{\mathcal{B}^{5/2}} x\right) - 1\right], \qquad (4.28)$$

and we observe that the effective curvature to apply to the outer solution is $-p_0/\delta^3$.

This completely determines the problem, and we are left with the effective outer problem:

$$-\delta^3 H_{xxx} = \mathcal{R}(H; h_\infty), \qquad (4.29a)$$

$$H(0) = 1, \quad H_{xx}(0) = -\frac{p_0}{\delta^3}, \qquad (4.29b)$$

$$H(1) = h(1), \quad H_x(1) = h_x(1), \quad H_{xx}(1) = h_{xx}(1), \qquad (4.29c)$$

which is solved similarly to the problem (4.26). Numerical solutions are shown in figure 6, which shows that the outer curvature H_{xx} tends to (different) non-zero values at the ends of the interval.

5. Asymptotic analysis of strong and weak surface tension

We now examine the limits of large and small inverse capillary number, $\delta^3 = \epsilon^3 \gamma/\mu U = 1/Ca$. The limit $\delta \to \infty$ corresponds to strong surface tension and/or slow motion of the substrate in which both the plate and the fluid uniformly tend towards a configuration with uniform height. In contrast, the limit $\delta \to 0$ corresponds to weak surface tension and/or fast motion of the substrate; this causes the film height to be uniform nearly everywhere except within a boundary layer near $x = 0$. In this section, we will find that the asymptotic results are similar to those found for a rigid plate by Trinh *et al.* (2014); however, when $\mathcal{B} \neq 0$ we will find that elastic effects introduce additional boundary layers near the edges of the plate that are crucial for the matching process (and the eventual determination of the far-field film height h_∞).
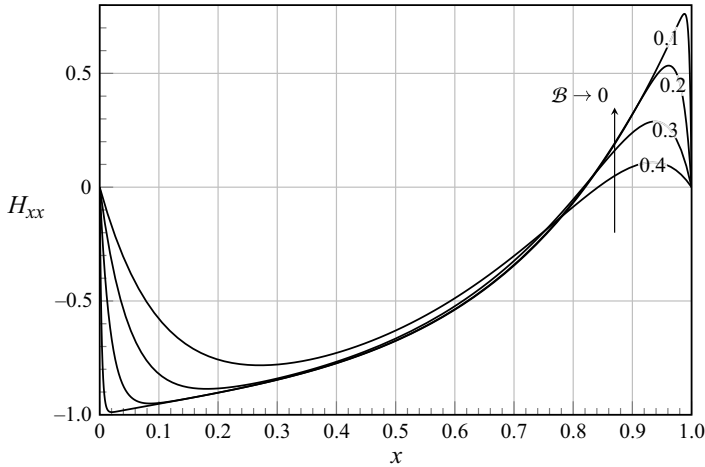
Figure 6. The curvature of the plate H_{xx} plotted as a function of x for various values of $\mathcal{B}$ in the case $\delta = 1$ and $p_0 = 1$. From top to bottom on the right, the curves correspond to $\mathcal{B} = 0.1, 0.2, 0.3$ and 0.4.

5.1. *The limit of slow substrate motion and/or strong surface tension, $\delta \to \infty$*

In the limit $\delta \to \infty$, it can be verified that both the height of the plate $H(x)$ and the height of the free surface $h(x)$ uniformly tend to unity. We then expand

$$H(x) = 1 + \sum_{n=1}^{\infty} \frac{H_n}{\delta^n}. \tag{5.1}$$

As in the corresponding analysis for the bending stiffness $\mathcal{B}$ described in §4, we are interested in developing a uniformly valid solution for the curvature of the plate H_{xx}, which is expected to be composed of boundary-layer solutions valid in inner regions near the ends of the plate, H_{xx}^{left} and H_{xx}^{right}, and an outer solution valid elsewhere, H_{xx}^{outer}. Also as in the previous analysis, if the prescribed pressure is zero, then there is no boundary layer at the left-hand end of the plate.

First, we consider the general case $p_0 \neq 0$. In the outer region $H \sim 1$ and $h_\infty \sim 1$, and assuming a dominant balance between the surface tension ② and pressure ③, we find that $\delta^3 H_{xxx} \sim 6$ and hence

$$H_{xx}^{\text{outer}} \sim \frac{1}{\delta^3}(6x - d) \tag{5.2}$$

for constant d. Notice that, unlike in §4.2, we do not assume that the curvature is $\mathcal{O}(1)$ in this limit.

In the left-hand boundary layer near $x = 0$, we seek a balance between elasticity ① and surface tension ② in (4.11), thus the boundary layer is of width $x = \mathcal{O}(\delta^{-3/2})$. Solving $\mathcal{B}^5 H_{xxxxx} \sim \delta^3 H_{xxx}$, and using the zero moment condition $H_{xx}(0) = 0$, we obtain

$$H_{xx}^{\text{left}} \sim -\frac{D}{\delta^3}\left[1 - \exp\left(-\frac{\delta^{3/2}x}{\mathcal{B}^{5/2}}\right)\right] \tag{5.3}$$

for a constant D. In order for this curvature to match the outer curvature (5.2), we take $\delta^{3/2}x \to \infty$ and thus require $D = d$. Moreover, imposing the pressure condition (2.17a) yields $D = p_0$.
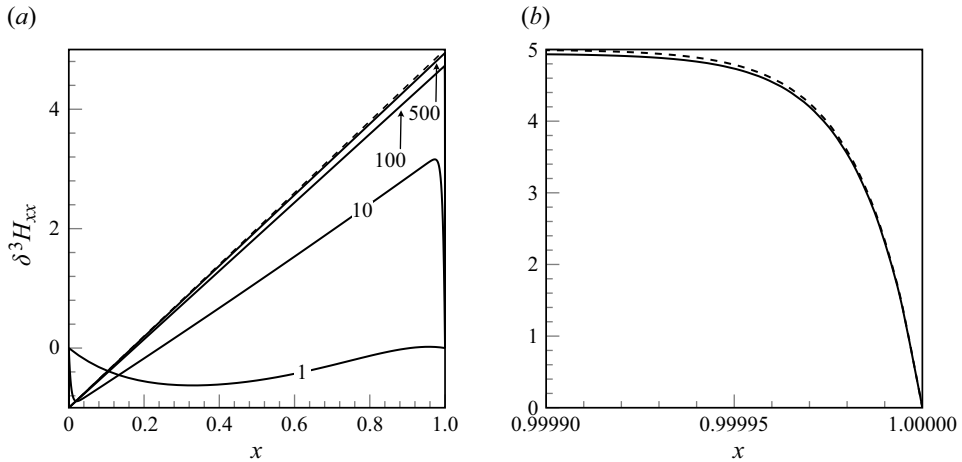
Figure 7. Plots of the re-scaled curvature of the plate $\delta^3 H_{xx}$ as a function of x for various values of δ in the case $\mathcal{B} = 0.5$ and $p_0 = 1$. From top to bottom on the right in (*a*), the curves correspond to $\delta = 500$, 100, 10 and 1. The asymptotic solution given by (5.5) for $\delta = 500$ is shown with the dashed line. Plot (*b*) is an enlargement of plot (*a*) near $x = 1$, including only the curves for $\delta = 500$ for clarity.

It remains to determine the curvature in the right-hand boundary layer near $x = 1$. Seeking a balance between elasticity ① and surface tension ② in (4.11) yields a boundary layer of width $1 - x = \mathcal{O}(\delta^{-3/2})$. Imposing the condition $H_{xx}(1) = 0$ yields

$$H_{xx}^{\text{right}} \sim \frac{E}{\delta^3} \left[1 - \exp \left(-\frac{\delta^{3/2}(1-x)}{\mathcal{B}^{5/2}} \right) \right], \tag{5.4}$$

where the constant E is determined to be $E = 6 - d = 6 - p_0$ once H_{xx}^{right} is matched to H_{xx}^{outer}. Thus we conclude that

$$H_{xx} \sim \begin{cases} -\dfrac{p_0}{\delta^3} \left[1 - \exp \left(-\dfrac{\delta^{3/2} x}{\mathcal{B}^{5/2}} \right) \right] & \text{for } x = \mathcal{O}(\delta^{3/2}), \\ \dfrac{1}{\delta^3}(6x - p_0) & \text{for } x \in (0, 1), \\ \dfrac{6 - p_0}{\delta^3} \left[1 - \exp \left(-\dfrac{\delta^{3/2}(1-x)}{\mathcal{B}^{5/2}} \right) \right] & \text{for } x = 1 - \mathcal{O}(\delta^{-3/2}). \end{cases} \tag{5.5}$$

Figure 7 shows the re-scaled curvature $\delta^3 H_{xx}$ for $\delta = 1$, 10, 100, 500, together with the nearly visually indistinguishable asymptotic solution given by (5.5) for $\delta = 500$. Note that we plotted $\delta^3 H_{xx}$ rather than H_{xx} in order to remove the algebraic dependence on δ.

With the curvature of the plate determined, we are now free to proceed similarly to the study of a rigid plate by Trinh *et al.* (2014) and investigate the Landau–Levich equation (2.6) in the limit $\delta \to \infty$. In this limit, the deviation from $h \sim 1$ for finite x is exponentially small in δ, so we seek a re-scaling near the the right-hand edge of the plate at $x = 1$. Setting $x = 1 + \delta X$, we substitute $h = 1 + h_1(X)/\delta + \mathcal{O}(1/\delta^2)$ and $h_\infty = 1 + h_{\infty 1}/\delta + \mathcal{O}(1/\delta^2)$ into the re-scaled Landau–Levich equation given by $h_{XXX} = 3(h_\infty - h)/h^3$. Solving the equation at $\mathcal{O}(1/\delta)$, we set the two integration constants to zero to remove the exponentially growing modes (see [8,9] in table 1), and match the heights of the free surface and the plate, $h_1(X = 0) = H_1(x = 1)$, where H_1 is from the series expansion (5.1).
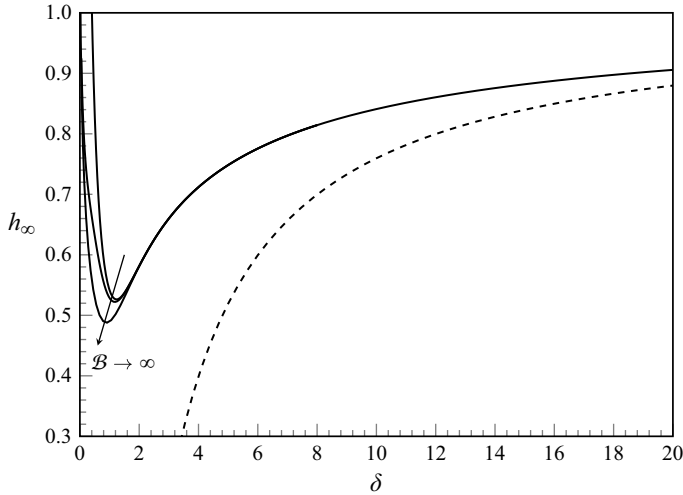
Figure 8. The far-field film height h_∞ plotted as a function of δ in the case $p_0 = 1$. From top to bottom, the curves correspond to $\mathcal{B} = 0.2, 0.5$ and 1. The two-term asymptotic approximation in the limit $\delta \to \infty$ given by (5.7) is shown with the dashed line.

Written in terms of x, this yields

$$h_1 = h_{\infty 1} + [H_1(1) - h_{\infty 1}] \exp\left(-\frac{3^{1/3}(x-1)}{\delta}\right). \tag{5.6}$$

From (5.5), we observe that the $\mathcal{O}(1/\delta)$ contribution to the plate is identically zero, $H_1 \equiv 0$, thus the free-surface correction in (5.6) depends only on $h_{\infty 1}$. Consequently, (5.6) yields an expression for the leading-order free-surface curvature near the edge of the plate given by $h_{xx}(1) \sim -3^{2/3} h_{\infty 1}/\delta^3$. The normal load at the edge of the elastic plate is $\mathcal{B}^5 H_{xxxxx}(1) \sim (p_0 - 6)/\delta^3$, which follows from (5.5). Finally, the fluid pressure and the load on the plate are related through (2.17b). Solving for the far-field film height gives

$$h_\infty = 1 + \frac{p_0 - 6}{3^{2/3}\delta}, \tag{5.7}$$

which is verified in figure 8.

The above results, and, in particular, the separation of the curvature H_{xx} into the three regions in (5.5), correspond to the situation in which there is a non-zero prescribed pressure $p_0 \neq 0$. If $p_0 = 0$, then the asymptotic structure is simpler and the outer solution with $H_{xx} \sim 6x/\delta^3$ applies all the way to $x = 0$ and satisfies the necessary zero moment condition. The limit $p_0 \to 0$ is regular: the above analysis, now consisting of only a single boundary layer near $x = 1$, is otherwise unaltered, and the results are consistent with setting $p_0 = 0$ in the previously derived formulae.

5.2. *The limit of fast substrate motion and/or weak surface tension, $\delta \to 0$*

In the limit $\delta \to 0$, the plate uniformly tends to unit height, $H \sim 1$, while the downstream height of the fluid tends to $h \sim h_\infty \sim 1/2$, except near the plate, where the free surface rises rapidly to match the edge of the plate. In terms of the analysis for the elastic plate, the principal difference between the limit $\delta \to 0$, the limit $\delta \to \infty$ of §. 5.1, and the limit $\mathcal{B} \to 0$ of § 4.2 is that for the case here, the $\delta \to 0$ limit is regular and there are no boundary layers. We thus expand as usual as $H = 1 + \delta H_1 + \mathcal{O}(\delta^2)$ and $h_\infty = 1/2 + \delta h_{\infty 1} + \mathcal{O}(\delta^2)$.
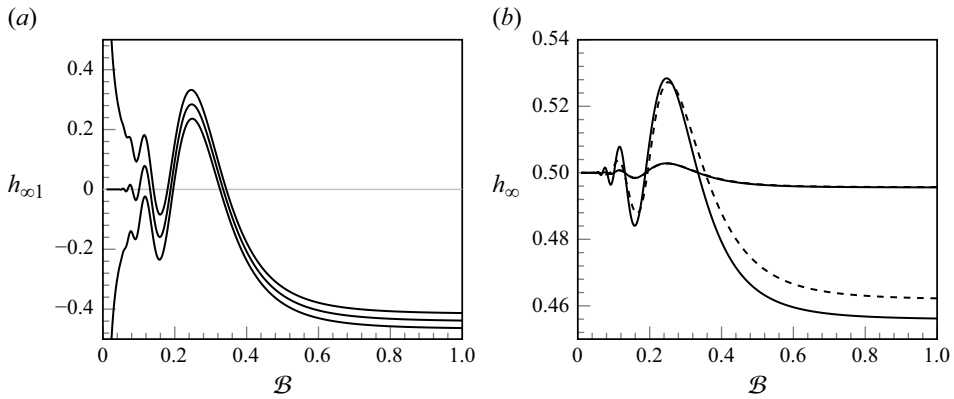
Figure 9. (*a*) The far-field height correction $h_{\infty 1}$ defined by $h_\infty = 1/2 + \delta h_{\infty 1} + \mathcal{O}(\delta^2)$, plotted as function of $\mathcal{B}$. From top to bottom, the curves correspond to $p_0 = 0.1$, 0 and -0.1. (*b*) The full numerical solutions for h_∞ in the case $p_0 = 0$ for $\delta = 0.1$ and $\delta = 0.01$ (shown with the solid lines) and the two-term asymptotic solution given by $1/2 + \delta h_{\infty 1}$ (shown with the dashed line) plotted as functions of $\mathcal{B}$. The pair of solid and dashed curves with the larger deviation from $h_\infty = 0.5$ corresponds to $\delta = 0.1$, and the pair of solid and dashed curves with the smaller deviation (which are nearly visually indistinguishable) corresponds to $\delta = 0.01$.

At $\mathcal{O}(\delta)$ in (2.11), we find $\mathcal{B}^5 H_{1xxxxx} = 6(H_1 - 2h_{\infty 1})$, which has the general solution

$$H_1(x;\ h_{\infty 1}) = 2h_{\infty 1} + \sum_{j=0}^{4} C_j \exp\left(\frac{6^{1/5} e^{2\pi i k/5} x}{\mathcal{B}}\right), \qquad (5.8a)$$

with constants C_j for $j = 0, \ldots, 4$. The values of the six unknowns $C_0, \ldots, C_4$ and $h_{\infty 1}$ can be determined by imposing the six boundary conditions

$$H_1(0) = 0, \quad H_{1xx}(0) = 0, \quad H_{1xxx}(0) = \frac{p_0}{\mathcal{B}^5}, \qquad (5.8b)$$

$$H_{1xx}(1) = 0, \quad H_{1xxx}(1) = 0, \quad H_{1xxxx}(1) = -\frac{h_{0xx}(1)}{\mathcal{B}^5}. \qquad (5.8c)$$

The only unknown in the above set of boundary conditions is the value of $h_{0xx}(1)$. This value can be found by numerically solving the Landau–Levich equation (2.6), starting at a large value of x and stopping once $h(1) \sim h_0(1) = 1$ is reached. Based on the results of Trinh *et al.* (2014), this value is approximately

$$h_{0xx}(1) \sim \frac{1.7639}{\delta^2}. \qquad (5.9)$$

In figure 9(*a*), we display the values of $h_{\infty 1}$ for $p_0 = 0.1$, 0 and -0.1, calculated using the above approach (i.e. solving (5.8)). In figure 9(*b*), we compare the two-term asymptotic solution $1/2 + \delta h_{\infty 1}$ with the full numerical solution for $\delta = 0.1$ and $\delta = 0.01$ when $p_0 = 0$. The figure confirms that there is good agreement between the numerical and asymptotic results; by $\delta = 0.01$ the curves are nearly visually indistinguishable.

There is, in fact, an additional distinguished limit when both $\mathcal{B} \to 0$ and $\delta \to 0$ simultaneously, which produces the increasingly rapid oscillations visible in figure 9. In the analysis leading to the asymptotic solution (5.8), $\mathcal{B}$ was assumed to be fixed while $\delta \to 0$. However, we note that the solutions that correspond to (afterwards) setting $\mathcal{B} \to 0$ have $H_1(1) \to -\infty$, and are thus inadmissible as soon as $H_1(1)$ exceeds $\mathcal{O}(1/\delta)$
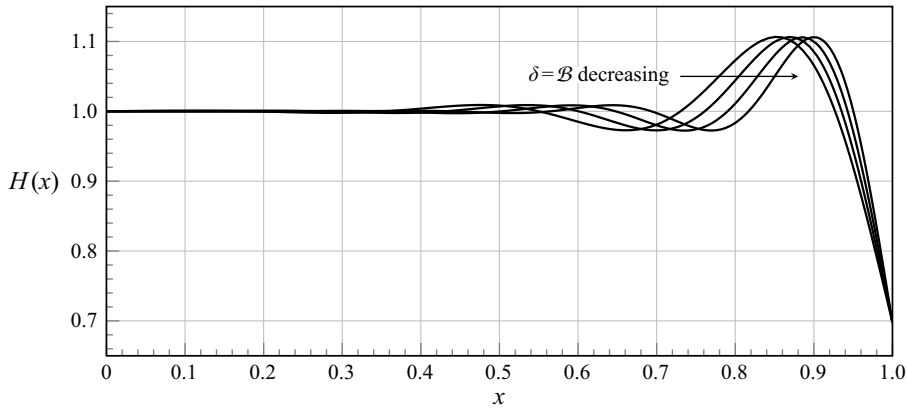
1007 A79-20

Figure 10. The height of the plate $H(x)$ plotted as a function of x for various values of $\mathcal{B}$ in the case $p_0 = 0$ and $\delta = \mathcal{B}$. From left to right, the curves correspond to $\delta = \mathcal{B} = 0.0735$, 0.0652, 0.0573 and 0.0500. There are further minima and maxima at smaller values of x not visible on the scale of the diagram.

in magnitude. Examples of solutions in this limit are given in figure 10. We observe that as $\mathcal{B} \to 0$ and $\delta \to 0$, H exhibits a series of maxima and minima in x, for which the primary maximum moves closer to the boundary at $x = 1$ in the double singular limits. The behaviour of these ripples seems to parallel that observed in the analyses of Wilson & Jones (1983), Snoeijer *et al.* (2008), Benilov *et al.* (2010) and McKinlay *et al.* (2023); we leave this particular special limit as an open problem.

6. Discussion

We have presented a numerical and asymptotic analysis of a mathematical model for a pinned elastic plate lying on the surface of a thin film of viscous fluid on a moving horizontal substrate. The system is governed by a third-order Landau–Levich equation for the height of the film and a fifth-order Landau–Levich-like beam equation for the height of the plate. In addition, an unknown eigenvalue (namely the far-field height) must be solved for. Nine boundary conditions close the system, which models the completing effects of elasticity, viscosity, surface tension and fluid pressure.

Four asymptotic limits were studied: the limits of large and small plate bending stiffness, and the limits of strong and weak surface tension. With the exception of the limit of large bending stiffness, $\mathcal{B} \to \infty$, in which the plate becomes rigid, the other three limits require matched asymptotic expansions in order to capture the singular effects at the edges of the plate. The occurrence of such boundary-layer effects is often the culprit for non-convergence of numerical solutions; we expect this to be a generic phenomenon for singularly perturbed elastocapillary problems.

We note that there are numerous connections between the well-known third-order Landau–Levich equation (2.6), which is commonly encountered in the modelling of coating flows, and the fifth-order Landau–Levich-like equation (effectively a beam equation but with a Reynolds equation embedded within it to provide the fluid flux and pressure). Thus many of the asymptotic and numerical approaches and results that arise in the study of the Landau–Levich equation have analogous approaches and results for the beam equation. For instance, a clear connection exists between the development of an apparent curvature in the outer solution in the limits $\mathcal{B} \to 0$ and $\delta \to \infty$ (see figures 5–7) and the analysis of moving contact lines, where the goal is to develop an
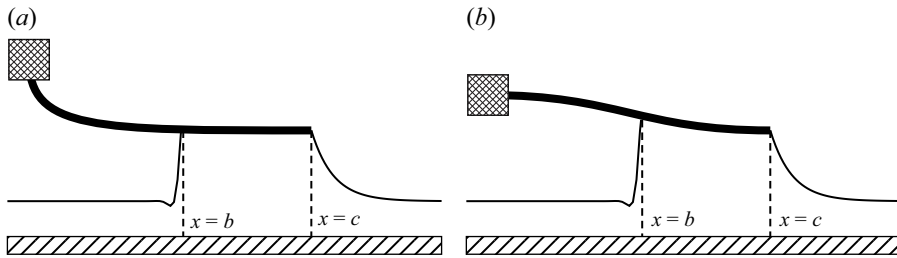
Figure 11. Sketches of two examples of flows with free contact points, $x = b$ and $x = c$, that must be determined as part of the solution. (*a*) A vertically clamped plate and (*b*) a horizontally clamped plate; in both examples, the plate is held stationary and the substrate is moved to the right with constant speed.

apparent or macroscopic contact angle (see, for example, Dussan & Davis 1974; Hocking 1981; Ren *et al.* 2015), related to an inner region near the singularity.

The solutions that we have presented, particularly the variety of different asymptotic regimes, exhibit a fascinating complexity; it is interesting to consider what other solutions exist when the physical set-up of the problem is modified, i.e. to consider the global bifurcation structure of the space of solutions (as controlled by parameters such as $\mathcal{B}$ and δ). As noted in §1, nonlinearity in the associated differential equations is often accompanied by non-uniqueness of solutions. The existence or non-existence of solutions, for the case of a rigid plate lying on a thin fluid film, was discussed by Moriarty & Terrill (1996) and Trinh *et al.* (2014). Rigorous results can be established for the case of a rigid plate (as was done by McLeod 1996), but the analogous theory remains unresolved for the much more complex boundary-value system that we have presented here. The non-uniqueness of the fifth-order beam equation (though uncoupled from another thin-film equation) was also noted by Dixit & Homsy (2013).

There are numerous interesting directions that we can highlight for future work. One variation of the problem presented here is inspired by the work of Seiwert *et al.* (2013), who studied the case of a vertically clamped plate, used within the blade coating system sketched in figure 11(*a*). For such geometries, it may not be possible to assume that the deformation of the plate from the horizontal is small, even though linear plate theory can still be used as a function of the plate arc length. Alternatively, one could consider a configuration with a horizontally clamped plate as sketched in figure 11(*b*), which will be more similar to the theory that we have presented in the present work. Note that in order to preserve the applicability of lubrication theory, it must be assumed that the plate is sufficiently flat during contact. Moreover, a particular challenge in studying such configurations is a consequence of the upstream connection point being *a priori* unknown and having to be determined as part of the solution. It is interesting to consider the parameter regime involved in these experiments. Specifically, Seiwert *et al.* (2013) considered a situation with $U \approx 8.2\,\text{mm s}^{-1}$, $\mu = 17.4\,\text{N m}^{-1}\,\text{s}^{-1}$, $L = 0.04\,\text{m}$, $\gamma = 0.02\,\text{N m}^{-1}$, and typical fluid depths of the order of $4 \times 10^{-3}\,\text{m}$. In the present non-dimensional parameters, this corresponds to $\delta^3 = Ca^{-1} \approx 10^{-4}$ and $\epsilon \approx 0.5 \times 10^{-1}$. Typical beam elasticity was $B = 4.2 \times 10^{-3}\,\text{N m}$, hence $\mathcal{B}^5 \approx 0.0184$. Note that $\epsilon^2/\delta^3 \approx 10^2$, so spatial variations in the tension in the plate may be significant, hence a more detailed mathematical model that includes some or all of the terms on the right-hand side of (2.8) may be required in order to fully capture the results of these experiments.

Many other more complicated variations of the present elastocapillary problem are possible, including systems on substrates with non-zero curvature (see, for example, Myers *et al.* 2002; Howell 2003; Jensen *et al.* 2004; Trinh *et al.* 2014). Following Seiwert *et al.*

(2013) there has been recent work by Krapez *et al.* (2020) (for Newtonian fluids) and Krapez *et al.* (2022) (for non-Newtonian fluids) who studied, experimentally, numerically and theoretically, the vertically clamped situation sketched in figure 11(*a*). Their analysis uses the experimental observations to judiciously simplify the mathematical model (see, in particular, the supplementary materials of Krapez *et al.* 2020); it would be interesting to apply the more complete asymptotic treatments that we have developed in the present work to the more challenging 'two-fluid' systems studied in such works. The situation of fully three-dimensional deflections also presents a fruitful playground for computational and analytical works. Although we have not considered the scenario here, we refer readers to the extensive review by Vella (2015) addressing the situation of three-dimensional interactions between fluids and elastic structures.

Declaration of interests. The authors report no conflict of interest.

Data availability statement. The data supporting the findings of this study are available within the paper.

REFERENCES

ASHMORE, J., HOSOI, A.E. & STONE, H.A. 2003 The effect of surface tension on rimming flows in a partially filled rotating cylinder. *J. Fluid Mech.* **479**, 65–98.

AUDOLY, B. 2011 Localized buckling of a floating elastica. *Phys. Rev. E* **84** (1), 011605.

BENILOV, E.S., CHAPMAN, S.J., MCLEOD, J.B., OCKENDON, J.R. & ZUBKOV, V.S. 2010 On liquid films on an inclined plate. *J. Fluid Mech.* **663**, 53–69.

BICO, J., REYSSAT, É. & ROMAN, B. 2018 Elastocapillarity: when surface tension deforms elastic solids. *Ann. Rev. Fluid Mech.* **50**, 629–659.

BICO, J., ROMAN, B., MOULIN, L. & BOUDAOUD, A. 2004 Adhesion: elastocapillary coalescence in wet hair. *Nature* **432** (7018), 690.

BRETHERTON, F.P. 1961 The motion of long bubbles in tubes. *J. Fluid Mech.* **10** (2), 166–188.

CRASTER, R.V. & MATAR, O.K. 2009 Dynamics and stability of thin liquid films. *Rev. Mod. Phys.* **81** (3), 1131–1198.

DE GENNES, P.-G., BROCHARD-WYART, F. & QUÉRÉ, D. 2004 *Capillarity and Wetting Phenomena: Drops, Bubbles, Pearls, Waves*. Springer.

DERJAGUIN, B.V. 1943 On the thickness of the liquid film adhering to the walls of a vessel after emptying. *Acta Physicochim. USSR* **20**, 349–352.

DIXIT, H.N. & HOMSY, G.M. 2013 The elastic Landau–Levich problem. *J. Fluid Mech.* **732**, 5–28.

DUPRAT, C. 2022 Moisture in textiles. *Ann. Rev. Fluid Mech.* **54**, 443–467.

DUPRAT, C., PROTIÈRE, S., BEEBE, A.Y. & STONE, H.A. 2012 Wetting of flexible fibre arrays. *Nature* **482** (7386), 510–513.

DUSSAN, E.B. & DAVIS, S.H. 1974 On the motion of a fluid–fluid interface along a solid surface. *J. Fluid Mech.* **65** (1), 71–95.

GIACOMIN, A.J., COOK, J.D., JOHNSON, L.M. & MIX, A.W. 2012 Flexible blade coating. *J. Coat. Technol. Res.* **9** (3), 269–277.

HEWITT, I.J., BALMFORTH, N.J. & DE BRUYN, J.R. 2015 Elastic-plated gravity currents. *Eur. J. Appl. Math* **26** (1), 1–31.

HOCKING, L.M. 1981 Sliding and spreading of thin two-dimensional drops. *Q. J. Mech. Appl. Math* **34** (1), 37–55.

HOSOI, A.E. & MAHADEVAN, L. 2004 Peeling, healing, and bursting in a lubricated elastic sheet. *Phys. Rev. Lett.* **93** (13), 137802.

HOWELL, P., KOZYREFF, G. & OCKENDON, J.R. 2009 *Applied solid mechanics*. *Cambridge Texts in Applied Mathematics*, vol. **43**. Cambridge University Press.

HOWELL, P.D. 2003 Surface-tension-driven flow on a moving curved surface. *J. Engng Maths* **45** (3), 283–308.

JENSEN, O.E., CHINI, G.P. & KING, J.R. 2004 Thin-film flows near isolated humps and interior corners. *J. Engng Maths* **50** (2), 289–309.

KRAPEZ, M., GAUTHIER, A., BOITTE, J.-B., AUBRUN, O., JOANNY, J.-F. & COLIN, A. 2022 Spreading of complex fluids with a soft blade. *Phys. Rev. Fluids* **7** (8), 084002.

KRAPEZ, M., GAUTHIER, A., KELLAY, H., BOITTE, J.-B., AUBRUN, O., JOANNY, J.-F. & COLIN, A. 2020 Impact of the wetting length on flexible blade spreading. *Phys. Rev. Lett.* **125** (25), 254506.

LANDAU, L. & LEVICH, B. 1942 Dragging of a liquid by a moving plate. *Acta Physicochim. URSS* **17**, 42–54.

LISTER, J.R., PENG, G.G. & NEUFELD, J.A. 2013 Viscous control of peeling an elastic sheet by bending and pulling. *Phys. Rev. Lett.* **111** (15), 154501.

MCKINLAY, R.A., WRAY, A.W. & WILSON, S.K. 2023 Late-time draining of a thin liquid film on the outer surface of a circular cylinder. *Phys. Rev. Fluids* **8** (8), 084001.

MCLEOD, J.B. 1996 Solution of a contact lens problem. *Eur. J. Appl. Math* **7** (6), 595–602.

MORIARTY, J.A. & TERRILL, E.L. 1996 Mathematical modelling of the motion of hard contact lenses. *Eur. J. Appl. Math* **7** (6), 575–594.

MYERS, T.G., CHARPIN, J.P.F. & CHAPMAN, S.J. 2002 The flow and solidification of a thin fluid film on an arbitrary three-dimensional surface. *Phys. Fluids* **14** (8), 2788–2803.

ORON, A., DAVIS, S.H. & BANKOFF, S.G. 1997 Long-scale evolution of thin liquid films. *Rev. Mod. Phys* **69** (3), 931–980.

PRANCKH, F.R. & SCRIVEN, L.E. 1990 Elastohydrodynamics of blade coating. *AIChE J.* **36** (4), 587–597.

QUÉRÉ, D. 1999 Fluid coating on a fiber. *Ann. Rev. Fluid Mech.* **31** (1), 347–384.

REN, W., TRINH, P.H. & WEINAN, E. 2015 On the distinguished limits of the Navier slip model of the moving contact line problem. *J. Fluid Mech.* **772**, 107–126.

SEIWERT, J., QUÉRÉ, D. & CLANET, C. 2013 Flexible scraping of viscous fluids. *J. Fluid Mech.* **715**, 424–435.

SINGH, K., LISTER, J.R. & VELLA, D. 2014 A fluid-mechanical model of elastocapillary coalescence. *J. Fluid Mech.* **745**, 621–646.

SNOEIJER, J.H. 2016 Analogies between elastic and capillary interfaces. *Phys. Rev. Fluids* **1** (6), 060506.

SNOEIJER, J.H., ZIEGLER, J., ANDREOTTI, B., FERMIGIER, M. & EGGERS, J. 2008 Thick films of viscous fluid coating a plate withdrawn from a liquid reservoir. *Phys. Rev. Lett.* **100** (24), 244502.

STONE, H.A. 2010 Interfaces: in fluid mechanics and across disciplines. *J. Fluid Mech.* **645**, 1–25.

TARONI, M. & VELLA, D. 2012 Multiple equilibria in a simple elastocapillary system. *J. Fluid Mech.* **712**, 273–294.

TRINH, P.H., WILSON, S.K. & STONE, H.A. 2014 A pinned or free-floating rigid plate on a thin viscous film. *J. Fluid Mech.* **760**, 407–430.

TUCK, E.O. & SCHWARTZ, L.W. 1990 A numerical and asymptotic study of some third-order ordinary differential equations relevant to draining and coating flows. *SIAM Rev.* **32** (3), 453–469.

VELLA, D. 2015 Floating versus sinking. *Ann. Rev. Fluid Mech.* **47**, 115–135.

WAGNER, T.J.W. & VELLA, D. 2011 Floating carpets and the delamination of elastic sheets. *Phys. Rev. Lett.* **107** (4), 044301.

WILSON, S.D.R. & JONES, A.F. 1983 The entry of a falling film into a pool and the air-entrainment problem. *J. Fluid Mech.* **128**, 219–230.